Journal of
Materials Chemistry B

ROYAL SOCIETY OF CHEMISTRY

PAPER

View Article Online
View Journal | View Issue

Cite this: *J. Mater. Chem. B*, 2026, **14**, 161

Lipid mapping of cell mitosis by non-covalent migratory fluorescence labelling

Anaïs C. Bourgès, * Massimiliano Garre and Donal F. O'Shea *

Received 29th August 2025,
Accepted 11th November 2025

DOI: 10.1039/d5tb01947h

rsc.li/materials-b

The concept of non-covalent migratory fluorescence labelling is introduced to spatially and temporally map intracellular lipids throughout a cell division cycle. This hands-off approach utilizes a small molecule BF_2-azadipyrromethene fluorophore, NM-ER, to first label the nuclear membrane and endoplasmic reticulum of cells at the interphase, which can migrate with the lipid components of these structures throughout mitosis as they disassemble, redistribute and reassemble prior to daughter cell separation. Through this unique approach to image capture, key prometaphase events such as lipid intrusion into the nucleus and nuclear membrane disassembly are observable, as are the stages of nuclear membrane reassembly in the telophase and lipid distribution during cytokinesis. When used alone, NM-ER can distinguish each phase of cell mitosis from lipid staining patterns, it is compatible with STED super resolution imaging, and, with an emission maximum of 648 nm, it is usable with other common GFP and nuclear DNA stains. The non-covalent NM-ER label remains associated with the originating lipid components as they undergo architectural reorganizations and changes in subcellular localization associated with mitosis. As lipid-based cell structures are influenced by numerous biological processes and mechanical forces, our approach to fluorescence imaging could offer novel perspectives into their different roles.

Introduction

Lipids, alongside amino acids, nucleotides and carbohydrates, are the underpinning building blocks of cells, though lipids differ in how they are employed in the construction of their higher order structures. Macromolecular proteins, DNA strands or polysaccharides are formed from cell programmed covalent bond formation, whereas in the case of lipids, a combination of weak van der Waals interactions, hydrophobic forces and phase separations drives the assembly of their higher ordered structures (without the formation of covalent bonds).[1] Another point of difference is that while lipids can be broadly grouped as phospholipids, glycerides, sphingolipids or sterols, they have structural diversity greater than that of the other biomolecular classes.[2] Cells produce tens of thousands of different lipid species performing key roles within membrane and organelle structures, in signaling, and in energy storage, making their study particularly challenging.[3] The dramatic breakdown and reforming of lipid comprised membrane structures, such as the endoplasmic reticulum (ER) and nuclear membrane (NM), that occurs during cell division can make this challenge even more pronounced.[4] Fluorescence microscopy and lipidomic mass spectrometry are two approaches often employed, which can give complementary information, with the former suitable for visualizing structures and the latter enabling the identification of specific lipids.[5]

Lipidomics has provided the ability to identify individual lipid species, but visualizing lipid dynamics remains a persistent challenge that could be addressed by fluorescence microscopy.[6] Most often, fluorescence labelling for microscopy is achieved through the direct covalent linkage (or strong specific binding) of a targeted molecular fluorophore or a genetically expressed fluorescent protein to a cellular feature of interest.[7] However, as lipids are relatively small molecules when compared to proteins, covalently linking them to a fluorescent probe could overly alter their molecular structure, thereby perturbing their natural functions and localization.[8] What remains relatively unexplored is the potential to utilize non-covalent fluorescence labelling of lipid based cellular structures to track their changes over time. Uniquely, this would require that the non-covalent labels remain associated with the components of the originating lipid structure as they undergo architectural reorganizations and changes of their subcellular localization. As lipid structures and localization are influenced by both biological processes and mechanical forces, such an imaging tool could offer a novel perspective on lipid behavior in live cells.

Despite their central importance, an understanding of lipid participation in pivotal biological events such as cell division

Department of Chemistry, RCSI, University of Medicine and Health Sciences, 123 St Stephen's Green, Dublin 2, Ireland. E-mail: donalfoshea@rcsi.ie, anaisbourges@rcsi.ie

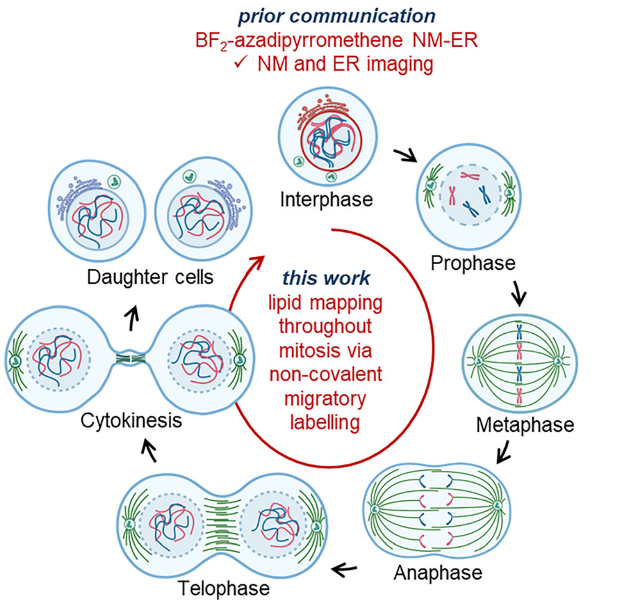

Fig. 1 Mapping of cell division phases through the recognizable changes in DNA and microtubules and in this work potentially through their associated lipid distribution patterns. This schematic represents the DNA and microtubular organization at different phases of cell mitosis from a cell in interphase to its division into two daughter cells. In this work, fluorophore NM-ER, which has been shown to non-covalently label lipids in the nuclear membrane (NM) and the endoplasmic reticulum (ER) of cells at the interphase (top cell), will be explored as a means of microscopy imaging of these lipids throughout mitosis by migratory fluorescence labelling.

remains underdeveloped.[9] Lipidomic mass spectrometry has provided key insights into the spatial and temporal identification of specific lipids regulated during cell division. Indeed, elegant studies by Eggert *et al.* revealed that lipid composition changes at different mitotic phases, suggesting that, for reasons not yet fully understood, specific lipids play distinct roles at different stages.[10] This is in strong contrast with the extensive knowledge of DNA and microtubular changes, which have been extensively studied (Fig. 1). In a similar manner, cell replication causes dramatic changes to lipid structures and spatial distribution during each phase of mitosis. At the outset of mitosis (interphase), the NM and ER are intact, yet they will entirely deconstruct during the pro(*meta*)phase, following which there are continuous lipid reorganizational changes through the anaphase and telophase, with the NM and ER both being fully reconstructed in time for the completion of cytokinesis. Previously reported approaches for the microscopy imaging of lipids during mitosis have employed fluorescent ER membrane bound proteins such as STIM1 and Sec61b.[11] In this work, we have developed the novel use of a single intracellular lipid favoring a molecular fluorophore to map the dramatic changes in lipidic structures throughout cell division.

In a recent study, we introduced the BF_2-azadipyrromethene fluorophore NM-ER, which non-specifically stains intracellular lipid membranes such as the NM and ER of interphase cells through non-covalent association with the lipids within these connected structures (Fig. 1, interphase cell image, prior work; Fig. 2, structure).[12] For the next stage of this work, the use of this fluorophore to follow the dramatic structural changes that occur to both the NM and ER during open mitosis in higher eukaryotes has been investigated.[13] As the NM and ER disassemble upon mitotic entry and reform upon completion to reestablish nucleocytoplasmic compartmentalization, it would be of significant value if these events could be tracked from start to finish using a single molecular probe. As such, if NM-ER remained associated with the dispersed lipids throughout the deconstruction and reformation of these structures, it would enable spatiotemporal mapping of their lipid distributions throughout cell mitosis (Fig. 1, this work). Once created, a mitotic lipid distribution map could complement existing DNA and microtubule markers, offering a less disruptive alternative that avoids potential fluorophore-induced toxicity associated with DNA and microtubule binding. Moreover, NM-ER is compatible with the super-resolution microscopy technique STED (stimulated emission depletion microscopy), so it could offer deeper insights into the roles of lipids during the complex sequence of events during cell division.[14]

Results and discussion

Characterization of the BF_2-azadipyrromethene fluorophore NM-ER for lipid imaging

The BF_2-azadipyrromethene fluorophore class has become increasingly popular in fundamental and applied imaging applications.[15] Advantageously, their emissions can be refined to meet specific needs, are highly photostable and have shown no toxicity issues when used *in vitro* or *in vivo*.[16] To achieve the imaging objective for NM-ER, it was designed to follow intracellular lipid structures by migrating alongside them as they undergo cellular reorganization (Fig. 2(A), schematic illustration). Structurally, NM-ER is overall charge neutral, has the simplest of BF_2 chelates and has α-pyrrole phenyl substituents for optimal emission wavelengths (Fig. 2). It exhibits only

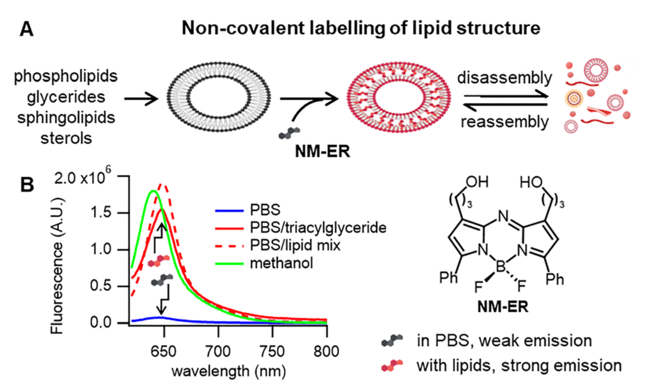

Fig. 2 Lipid responses of NM-ER. (A) Concept schematic of dynamic lipid structure imaging through non-covalent migratory fluorescence labelling. (B) Emission spectra of NM-ER at 5 μM in phosphate buffered saline (PBS, blue trace, λ_{max} 647 nm), in PBS/glyceryl trioleate (solid red trace, λ_{max} 648 nm), in PBS/L-α-phosphatidylcholine and cholesterol mixture (dotted red trace, λ_{max} 647 nm) and in MeOH (green trace, λ_{max} 638 nm) upon excitation at 590 nm. NM-ER structure and lipid fluorescence response.

moderate solubility in phosphate buffered saline (PBS), which is achieved through the inclusion of the two primary alcohol substituents at the β-pyrrole positions (Fig. 2(B)). As 1-alkanols are recognized to be highly effective at assembling inside lipid bilayers, with the hydroxyl group hydrogen bonded to the carbonyls of lipid headgroups, it was thought plausible that the bis-1-alkanols of NM-ER would favor accumulation within intracellular membranes such as ER and NM.[17] To illustrate the potential for this association, a comparison of the emission properties of NM-ER in PBS alone and in solutions containing the representative triacylglyceride glyceryl trioleate, or a mixed lipid system of L-α-phosphatidylcholine and cholesterol, was performed.[3c,18] As expected, a weak emission centered at 647 nm was recorded in PBS alone, and while both lipid-containing solutions showed a negligible change in wavelength emission maxima (648/647 nm), they had a 69- and 63-fold increase in intensity respectively (Fig. 2(B)). These initial results illustrated that when NM-ER is associated with aqueous lipid microenvironments, its emission is significantly enhanced, but the unknown question for this work is whether this association could be utilized to image lipid structures as they disassemble and reassemble during cell mitosis (Fig. 2(A)). If this proved to be the case, then the spatiotemporal image capture of lipid associated structures at each phase of mitosis could be image-able using a single molecular fluorophore.

Prolonged live cell imaging with NM-ER

To first determine if intracellular NM-ER emission could be sustained throughout mitosis, live cell experiments were conducted in which the progression from parent to daughter cells was imaged. Encouragingly, when 0.5 μM of fluorophore was added to HeLa Kyoto (HeLa) cells, it was found that emission was readily detected throughout each phase of the replication process, with the daughter cells each having comparable fluorescence intensity to the parent (Fig. 3 and Movies S1, S2, Fig. S1 for additional experiment with DNA co-stained). These prolonged 4 h timelapses in live cells indicated that NM-ER could be used to follow lipid-induced emission without impeding mitosis.

Interphase lipid membrane imaging with NM-ER

Next, for a more detailed analysis of lipid distribution throughout mitosis using NM-ER, the representative cancerous and macrophage cell lines HeLa, MDA-MB 231 (MDA) and RAW 264.7 (RAW) were employed. As previously reported for cells at the interphase, NM-ER stains several key lipidic structures including the NM and the ER.[12] Notably, at the interphase in all three cell lines, the NM was seen as a distinguishable line surrounding the nucleus and the ER staining pattern was of tubule-like structures with mitochondria also observed (Fig. S2). Prior literature, using cells expressing the fluorescent ER bound proteins YFP-STIM1 or GFP-Sec61β, has described ER lipid structures as either sheet- or tubule-like at the interphase and that an interconvertible continuum may exist between both forms.[19,20]

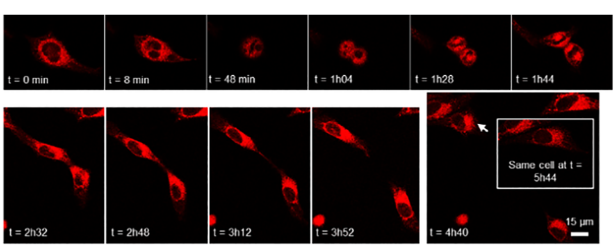

Fig. 3 Time lapse of NM-ER (0.5 μM concentration) fluorescence imaging of an individual HeLa Kyoto cell undergoing mitosis to form two daughter cells over 4 h. Confocal microscopy images acquired with a 20× objective (Movie S1).

Mapping lipids during mitosis

Initially, cells undergoing division were incubated with either NM-ER alone or co-stained with the DNA marker Hoechst. With images generated from NM-ER alone, each of the mitotic phases was clearly distinguishable from one another through their characteristic patterns of fluorescent lipid areas and lipid-free "negative spaces" (Fig. 4 and Movie S3 for 3D videos of each phase). Known features of mitosis could be gleaned from these images such as during the prophase, while the NM remains intact, the first ingress of a lipid tentacle into the nucleus can be observed originating from the NM. As the prophase progresses into the prometaphase and the NM breaks down, this lipid intrusion expands, forming a squid-like series of branched tubules interposed between the chromosomes (Fig. 4, prometaphase). In the metaphase, as the cells round up, lipids occupy the entire intracellular space except for the metaphase plate, where the chromosomes are lined up, giving a dumbbell-shaped outline (Fig. 4, metaphase). As sister chromatids are pulled apart in the anaphase, the interspace zone which is essentially free of lipids, enlarges in size, surrounded by lipids, resulting in the lipid-free negative space taking on a butterfly wing-shaped pattern (Fig. 4, anaphase). As the NM is reformed during the telophase, this interspace gradually fills with lipids as the cleavage furrow deepens. A lipid-free region is consistently observed at the poles of the two future daughter cells (opposite to the junction area) with a high concentration of lipids around the reforming nuclei. During cytokinesis, the lipid-rich intracellular bridge connects the near-separated daughter cells that resemble a pair of eyes as the chromatin discs at the center of each cell are surrounded by lipids (Fig. 4, cytokinesis). The DNA co-stain proved helpful to confirm the identity of each mitotic phase (prophase, prometaphase, metaphase, anaphase, and telophase) and cytokinesis of individual cells; however, with experience, the NM-ER pattern alone became sufficient to make this determination (Fig. 4 and Movie S3). With the phases clearly identified and distinguishable from each other, we next examined each in more detail to investigate dynamic changes to their lipid structural features.

Disassembly of the NM and ER during the prometaphase

Prometaphase is a transitional phase of mitosis characterized by the disassembly of the NM and ER, allowing spindle microtubules to access the condensed chromosomes.[4a,21] During this

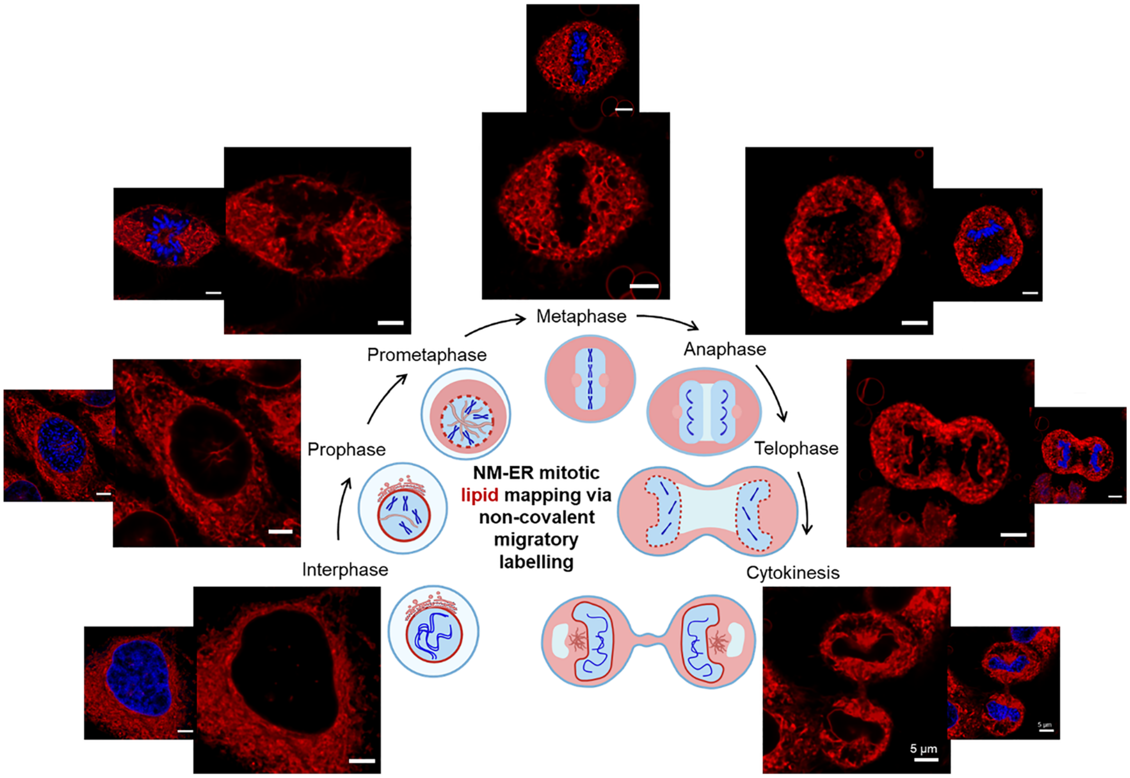

Fig. 4 Lipid mapping with NM-ER throughout cell mitosis by non-covalent migratory fluorescence labeling. Larger cell images show NM-ER (red) fluorescence patterns at each phase of cell mitosis. The smaller images correspond to the same cell with Hoechst co-registered DNA (blue). Cartoons illustrate the identifiable pattern shapes for lipids (red regions) for each phase, with DNA as dark blue colored regions and negative space areas with no fluorescence shown in grey. Scale bar 5 µm. 3D stacks of each mitotic phase can be visualized in Movie S3.

stage, kinetochore complexes form at the centromeric regions of each chromosome, serving as anchoring sites for spindle fibers originating from opposite centrosomes. Once attached, microtubules facilitate the movement of chromosomes toward the metaphase plate. Viewing the prometaphase from a lipid standpoint with confocal microscopy, the onset of mitosis can be distinguished by a tentacle-like intrusion of lipids, emanating from the NM, into the nucleus body. When co-stained with Hoechst, these lipid tentacles closely follow the contours of the condensed chromosomes prior to their migration to the metaphase plate (Fig. 5(A) and Movie S4, for other examples see Fig. S3). These intricate structures, together with the remaining sections of the NM, were better visualized with super-resolution STED imaging. This enhanced the resolution by a factor of three, providing a clearer view of both the origins of the lipids and the tubular network itself (Fig. 5(A)). The STED measurements of individual intruding tubules were comparable with the NM of an adjacent interphase cell (105 nm). While not apparent from the NM-ER images, it could be understood that the lipids alone could not exert the mechanical forces necessary to drive chromosome condensation and separation and that other non-lipid structures must be closely associated with these lipids (see later).

It could also be observed that as NM disassembly proceeded, in tandem the intranuclear lipid intrusion grew. The visual hallmark of this disassembly is that the NM surface loses its smooth, continuous appearance in the interphase, developing irregular contours and becoming disjointed. Fig. 5(B) shows an example 3D image of a section of continuous NM in a cell at the interphase stage, with a neighboring prometaphase cell in the same field of view being fenestrated and disjointed. By the completion of the prometaphase, all recognizable structural features of the NM and ER have disappeared, with their lipids dispersed as the metaphase emerges (Fig. S3).

Key cellular tasks during the metaphase and anaphase are the movement of chromosomes to the metaphase plate and their attachment to spindle microtubules *via* kinetochores. These microtubules originate from opposite centrosomes, ensuring bipolar attachment, which is essential for the equal distribution of genetic material. During the anaphase, motor protein shortening of the microtubules forces separation of the sister chromatids and they are pulled toward the opposite poles of the cell. Concurrently, the non-kinetochore microtubules elongate, pushing the cell poles further apart and contributing to cell elongation. Remarkably, the central region of the cell in which much of this activity occurs remains essentially devoid of lipids, whereas the outer circumference and regions surrounding the centrosomes have a concentration of densely packed lipids (Fig. S4). This gives the distinctive contrasting non-fluorescent regions (negative shapes) through which both the metaphase and the anaphase can be readily identified (Fig. 4).

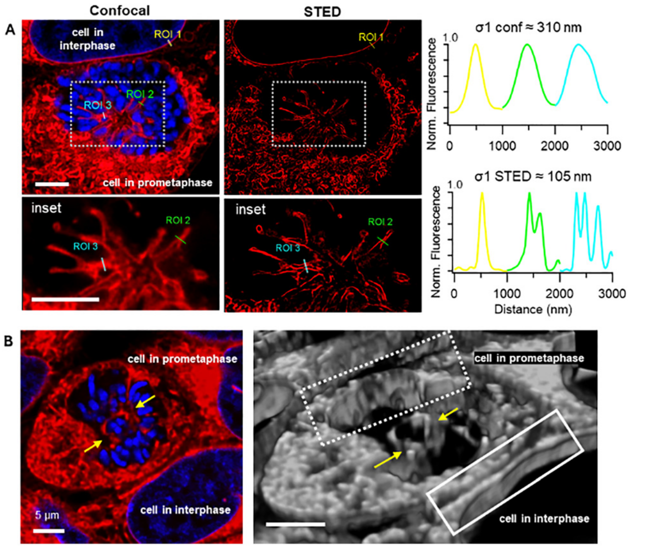

Fig. 5 Observing nuclear lipid intrusion and nuclear membrane disassembly during the prometaphase in HeLa cells. (A) Confocal and STED images of two cells, one in the interphase and one in the prometaphase, imaged with NM-ER (red) and DNA co-registered with Hoechst (blue). Early-stage lipid intrusions into the nucleus of the cell in the prometaphase are highlighted within boxes and shown as expansions below the full images. Comparative confocal and STED fluorescence intensity profiles of three different ROIs as indicated in the images (ROI 1 nuclear membrane of the interphase cell, ROI 2 and 3 nuclear lipid channels of the prometaphase cell); see Movie S4 for a 3D view and for images from additional experiments, see Fig. S3. (B) Single frame of a 3D reconstruction image of two cells, one in the interphase and one in the prometaphase, imaged with NM-ER (red) and DNA co-registered with Hoechst (blue) showing a section of disassembling nuclear membrane and lipid nuclear intrusion indicated by the yellow arrows (left image). For clarity, the NM-ER channel of the same two cells is shown in black and white, with the disassembling nuclear membrane of the prometaphase cell indicated within the dashed box and, as comparison, an intact nuclear membrane of the adjacent interphase cell within the solid box. Scale bars 5 μm.

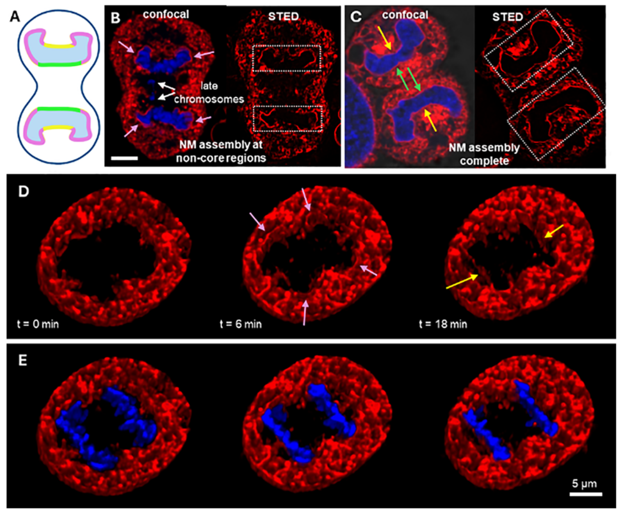

Fig. 6 Identification of the three periods of nuclear membrane reassembly around the chromatin discs in HeLa cells using NM-ER (red) with DNA co-stained with Hoechst (blue). (A) Cartoon showing non-core (purple), outer-core (yellow) and inner-core (green) chromatin disc regions. (B) Confocal and STED images of a cell showing partially reassembled NM (purple arrows in the confocal image and dashed boxes in the STED image) at the non-core regions of the chromatin discs. Late chromosomes are indicated by white arrows. (C) Confocal and STED images of a cell showing completely reassembled NM (yellow and green arrows in the confocal image and dashed boxes in the STED image) at both non-core and core regions of the chromatin discs. (D) Timelapse of confocal images over 15 min showing first the non-core assembly (purple arrows), followed by the outer-core assembly (yellow arrows) of the NM. (E) The same image sequence as in (D) with DNA co-stain included. Scale bars 5 μm. For images from additional experiments, see Fig. S4 and Movies S6–S8.

Reassembly of the NM during the telophase

Telophase, the reverse of pro(*meta*)phase, is the known cycle time point when the NMs begin to form around the separated chromatin discs, which will become the two future daughter cell nuclei. Importantly, with respect to the reassembly of the NM, previous reports have shown that there are three spatial edge regions of the chromatin discs, which are termed the inner and outer cores and non-core regions (Fig. 6(A), schematic).[22] It has been reported in the literature that NM formation may occur in either a synchronous or asynchronous manner, during which different sections of the membrane form in a specific temporal order. For example, in HeLa cells, an asynchronous assembly has been noted in which the membrane forms first at the non-core positions, then at the outer core and finally at the inner core.[22] Using NM-ER emission as a guide, HeLa cells in telophase were examined to detect evidence of this temporal regulation of NM formation. Through confocal and STED microscopy, cells were identifiable at each of the three steps of NE formation, confirming an asynchronous assembly around the chromatin discs for this cell line (Fig. 6 and Movie S6 for the associated 3D movies; for additional images, see Fig. S4). Timelapse microscopy of a single live cell over 20 min was employed to confirm that following membrane assembly in the non-core region, the outer-core was next to be addressed (Fig. 6(D), (E) and Movie S7). The late inner core formation has been attributed to microtubule detachment from the chromosomes prior to this section of the membrane being completed.[23] Remarkably, nuclear pore (NP) complexes were observable in the first assembled non-core membranes prior to completion of the core membrane regions through the use of the NP stain WGA-CF594 in fixed cells (Fig. S5). It is known that NP complexes can assemble concurrently with the membrane at the non-core chromatin disc positions, indicating that some lipid sub-structures used may contain preassembled NP complexes.[24] This study of lipids during the telophase underscores the potential for using NM-ER to observe the temporal regulation of membrane recruitment to the chromatin surface.

Lipid accumulation at the cleavage furrow during cytokinesis

Cytokinesis, as the final step of the cycle during which the cytoplasm divides to form two daughter cells, begins with the formation of a cleavage furrow during the telophase that deepens until the parent cell is pinched into two separate cells.[25] Lipids are known to play multifaceted roles in cytokinesis,

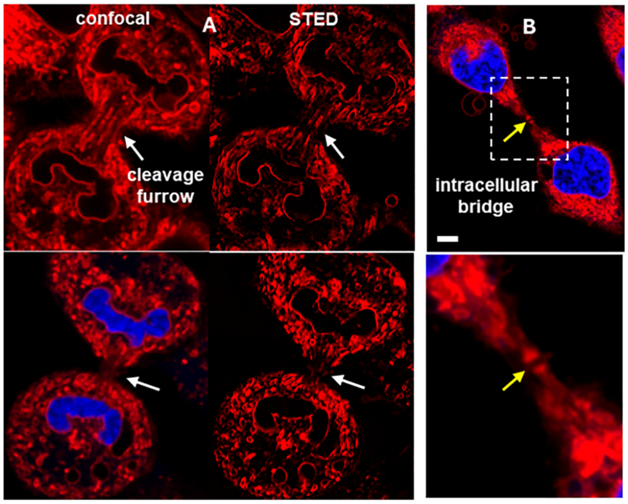

Fig. 7 Confocal and STED image capture of lipids during cytokinesis in HeLa cells using NM-ER (red) with DNA co-stained with Hoechst (blue). (A) Representative confocal and STED images of a cell at early cytokinesis with a completed NM and lipid accumulation at the cleavage furrow (white arrows). (B) Confocal images of a cell at late cytokinesis with distinctive lipid accumulation at the intracellular bridge (boxed area) and with midbody indicated (yellow arrows), with lipids flanking the midbody shown in an expanded view of the boxed area. Scale bars 5 μm. Movie S9 and Fig. S6 for additional examples.

particularly in membrane remodeling, signaling, and the mechanical stability of dividing cells.[26] As was the case for each phase of mitosis, NM-ER emission persisted into cytokinesis with the lipid contents of the cytosol, the fully reassembled NMs, and the cleavage furrow clearly visible (Fig. 7(A), for 3D *z*-stack see Movie S9).

The midbody is a microtubule-rich structure that forms in the intercellular bridge between the two daughter cells during late cytokinesis and plays a pivotal role in orchestrating the final abscission event.[27] Examination of NM-ER images acquired nearing the final moments prior to abscission showed the accumulation of lipids on either side of the midbody which itself could be recognized as a dark zone situated between these two concentrated lipid areas (Fig. 7(B), for 3D *z*-stack see Movie S9).

Co-registering NM-ER with microtubules during mitosis

Microtubules play a crucial role in ensuring accurate chromosome segregation during cell mitosis. These dynamic, cylindrical structures, composed of α- and β-tubulin dimers, assemble into the mitotic spindle, which is responsible for aligning and separating the chromosomes.[28] At each phase of cell replication, they exert distinct pushing and pulling mechanical forces generated by their ability to rapidly grow (polymerize) and shrink (depolymerize). Following mitotic spindle disassembly, a subset of microtubules reorganize into the central spindle and midzone

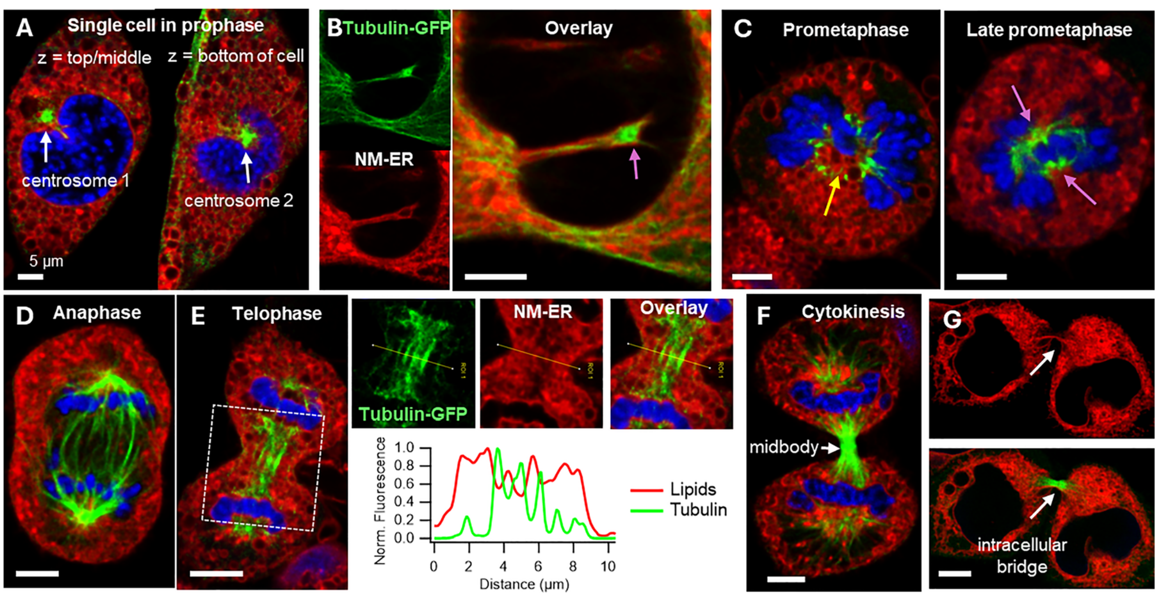

Fig. 8 Co-registration of lipids with microtubules (tubulin-GFP) at different cycle phases of mitosis and cytokinesis. HeLa cells expressing tubulin-GFP (green) with Hoechst labelled DNA (blue) and NM-ER labelled lipids (red). (A) Two images of a single cell in the prophase at different *z* positions showing the two centrosomes connected by microtubules and lipids. (B) Expanded view of microtubules surrounded by lipids with one cell centrosome in view. (C) Images of two different cells in the prometaphase; on the left, the intrusion of lipids into the nucleus is closely associated with the centrosomes, the spindle forming regions and between chromosomes. The right cell image shows that the forming spindles and associated centrosomes are surrounded by lipids. (D) Cell in the anaphase with lipids mostly confined to the cell peripheral regions with the interspace being relatively devoid of lipids. (E) Cell in the telophase showing lipids in close association with microtubules within the cleavage furrow, with the insets showing expanded views of tubulin-GFP and NM-ER images of the boxed cell area, and fluorescence intensity profile plots of the ROI line showing overlapping association of microtubules and lipids. (F) Cell in cytokinesis showing lipid, DNA and microtubule distribution in the daughter cells and the midbody closely abutted to the plasma membrane of the intercellular bridge between the cells. (G) Illustration using NM-ER only (top), and together with tubulin-GFP (bottom), of the presence of lipids within the intracellular bridge during cytokinesis. Scale bars 5 μm.

to control the cleavage furrow and guide membrane trafficking events essential for the final physical separation of daughter cells during cytokinesis.[29] As such, the association between lipids and microtubules is of fundamental interest as lipids balance intracellular forces and microtubules exert dynamic forces critical to cell division.

In order to co-register NM-ER stained lipids with microtubules and centrosome boundaries, CellLight tubulin-GFP (a fusion construct of human tubulin and emGFP) was used to stain tubulin in a live cell compatible manner.[30] Notably, while lipids and centrosomes were closely associated throughout mitosis, microtubules varied according to the mitotic phase. Upon examination of cells co-stained with NM-ER and tubulin-GFP, it became apparent that centrosomes resided within a pocket of lipids which was most apparent in the prophase and metaphase (Fig. 8(C)).

The first lipid intrusions into the nucleus detected by NM-ER in the prometaphase occur in regions near the centrosomes, where the accompanying microtubules are also enclosed by lipids (Fig. 8(A), (B) and Movie S11). As the nuclear intrusion of lipids grows throughout the prometaphase, this was closely associated with the expansion of microtubules into the nucleus, where attachment to the chromosomes occurs (Fig. 8(C) and Movie S11). During the metaphase and anaphase, microtubules extend into the interspace between the two centrosomes; however, this central region is essentially devoid of lipids while the centrosomes themselves remain surrounded by lipids (Fig. 8(D)). As the cleavage furrow emerges and deepens during the telophase, lipids infiltrate the interspace and have close spatial proximity to the microtubules, as confirmed by line intensity emission profiles for both fluorophores (Fig. 8(E)). As expected, cells in cytokinesis had a high concentration of microtubules through the intercellular bridge between the daughter cells with NM-ER showing the presence of surrounding lipids (Fig. 8(F), (G) and Movie S11).

Co-registering NM-ER with mitochondria during mitosis

Mitochondria change shape and outer lipid membrane components during mitosis, so it was considered likely that NM-ER could also stain their outer membranes. Published studies have shown that mitochondrial distribution is regulated by the microtubule cytoskeleton during division and that their distribution changes with each phase.[31] To investigate the lipid/mitochondria relationship, HeLa cells at each phase of mitosis were co-stained with NM-ER and Mito-Tracker green and the distribution of both was examined (Fig. S7). Specifically, mitochondria were not observed in many active lipid areas such as the nuclear lipid intrusions of the prometaphase or surrounding centrosomes during the metaphase/anaphase, nor in the reforming NM during the telophase. In the metaphase, the mitochondria were observed in the cytoplasm around the metaphase plate, though excluded from the central region of the cell, while in the telophase, they were in the cleavage furrow and during cytokinesis in the intracellular bridge, which is consistent with previous reports.[32]

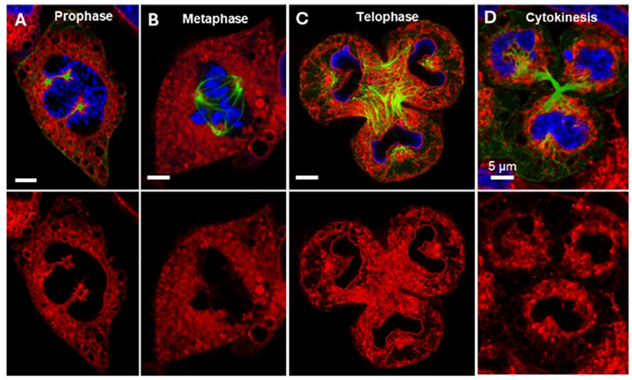

Fig. 9 Imaging of tripolar mitosis using NM-ER (red), CellLight tubulin GFP (green) and Hoechst (blue). Images of tripolar HeLa cells co-registered with DNA (blue), microtubules (green) and lipids (red) in the top panels and the same cells showing NM-ER alone in the bottom panels for the (A) prophase, (B) metaphase, (C) telophase and (D) cytokinesis. For 3D z-stacks, see Movie S12. Scale bars 5 μm.

NM-ER advantage over DNA staining in live cell imaging

In cultured HeLa cells, aberrant tripolar mitotic cells were occasionally observed during live cell experiments.[33] As DNA binders such as Hoechst are known promoters of tripolar mitosis, we took advantage of NM-ER to examine lipid distributions during this abnormal cell division.[34] In such multipolar divisions, the lipid distributions through each phase, as marked by NM-ER, were like that of a normal bipolar division, albeit in triplicate. In the prophase, three lipid-surrounded centrosomes were observed, which progressed through chromosome separation in the metaphase and NE reassembly occurring in the telophase (Fig. 9(A)–(C) and Movie S12). Finally, upon entering cytokinesis abscission resulted in the production of three daughter cells (Fig. 9(D)).

Conclusions

Using non-covalent fluorescence labelling strategies offers exciting opportunities for cell imaging as they reduce fluorophore complexity by eliminating the need for reactive functional groups and are relatively easy to use (Fig. 10). However, successful labelling requires partnership with the cell since it controls the intracellular positioning of the fluorophores. Non-covalent approaches have found particular utility for staining plasma membranes through transitory labelling before fluorophore internalization.[5b,35] They have also found uses for labelling lysosomes in which a fluorophore becomes entrapped within the acidic vesicles, and lipid droplets in which highly lipophilic compounds accumulate.[36,37] Yet, this approach has seen much less use in the labelling of intracellular organelle membranes of mitochondria, the ER and the NM.[12,38]

Cells produce thousands of different lipid species performing key roles within membrane and organelle structures, in signaling, and in energy storage, making their study particularly challenging as they are not amenable to covalent fluorophore labelling. In this study, we expanded the non-covalent

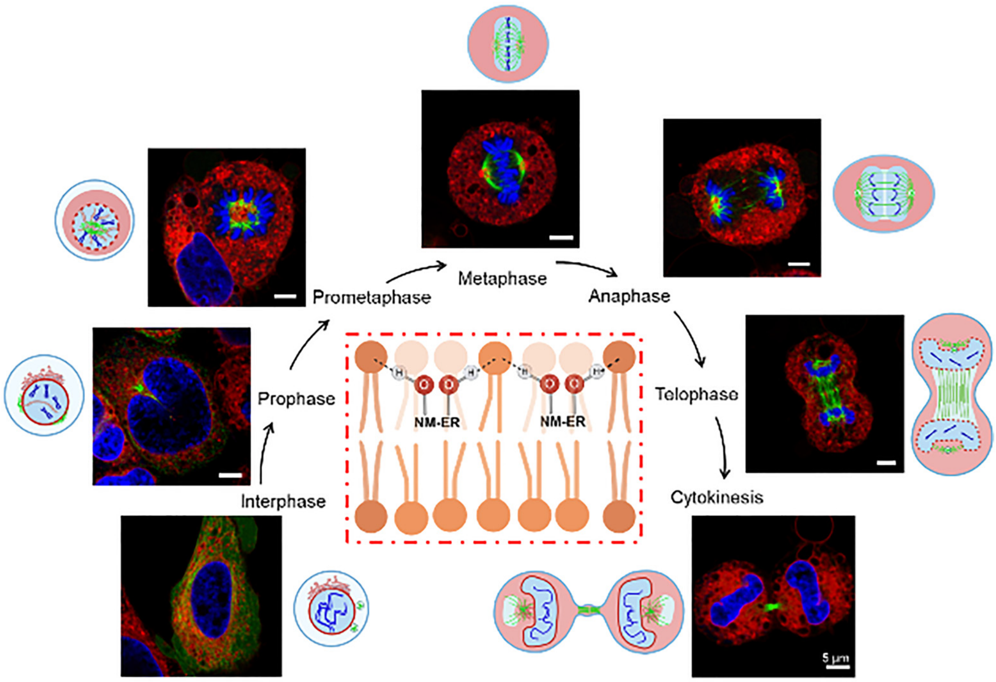

Fig. 10 Mitotic mapping of lipids with NM-ER summary including co-registration with DNA and microtubules. Representative fluorescence images of HeLa cells with NM-ER (red), Hoechst (blue) and tubulin-GFP (green) and a schematic representation of each cell division phase. For 3D cell views, see Movie S13. Scale bar 5 μm. For additional experiment images, see Fig. S8. Inset (dashed red box): Potential for hydrogen bonding from aliphatic alcohol functional groups of NM-ER to lipid head groups.

labelling to the concept of migratory labelling, as the initial structures labelled are not permanent and undergo deconstruction and reconstruction through normal cell division. This places an additional challenge on the fluorophore to remain with the lipid components, without covalent linkage, of the original structures throughout cell division changes. To achieve this aim, the fluorophore NM-ER has been engineered to bypass accumulation in the plasma membrane in favor of the internal membranes of the ER and NM, with limited accumulation in lipid droplets. This was achieved through the inclusion of two primary aliphatic alcohol groups on the non-charged fluorophore. The lack of charge inhibits accumulation within the plasma membrane, while the alcohol groups offer the potential for hydrogen bonding within intracellular membranes. Purposefully, this accumulation does not exhibit preferential affinity toward any particular lipid species. A contributing factor to NM-ER's migratory abilities may be that as an aliphatic diol it forms hydrogen-bonded networks which connect neighboring lipid head groups within the membrane (Fig. 10, red box inset). Such hydrogen bonds are known for aliphatic alcohols and networks have been reported for simpler diols.[39] Besides, it should be noted that the potential for NM-ER redistribution independent of lipid movement does exist. Despite the well-known changes in DNA and microtubular structures during mitosis, systematic monitoring of lipid changes is relatively unexplored. A lipid mapping could provide insights into how their distributions respond to biological stimuli and mechanical forces during normal and abnormal division events. With the use of NM-ER as a non-covalent migratory lipid marker, this can now be achieved with key lipid features observable, including their association with microtubules, chromatin discs and mid-body, from this single molecular fluorophore, negating the need for cell transfections or antibodies. By using this soft, non-invasive approach, we shadow the cells' own machinery that redeploys lipids throughout mitosis as the structures from which they are built disassemble and reassemble. As the NM-ER fluorophore wavelengths are compatible with other common nuclear and GFP stains, it is possible to position lipids spatially and temporally relative to DNA and microtubules. In intracellular lipid research, NM-ER's just-add-and-image ease of use, along with its suitability for time-lapse live or fixed cell imaging and confocal, widefield, or STED microscopy, should allow for its widespread application.

Methods

In solution measurement

5 μM of NM-ER was diluted in methanol or water (from a high concentration of fluorophore in methanol) or lipid mixtures obtained from a liposome kit (L4395, Sigma-Aldrich). NM-ER was synthesized as previously reported.[12]

Cell culture

HeLa Kyoto, RAW 264.7 and MDA-MB 321 cells were cultured in Dulbecco's Modified Eagle's Medium (DMEM), supplemented with 10% fetal bovine serum (FBS), 1% L-glutamine, and penicillin/streptomycin (1000 U mL^{-1}), and incubated at 37 °C and 5% CO_2. Cells were seeded on an eight-well chamber slide (Ibidi) at a density of 1×10^4 cells per well for 48 to 72 h (about 80% confluency).

Image acquisition

As previously described, images were acquired on a Leica Stellaris 8 Falcon microscope REF. Live cell imaging experiments were carried out at 37 °C and 5% CO_2. Images were acquired using a Leica HC PL APO CS2 100×/1.40 oil immersion objective (unless specified) with excitation at 594 nm for NM-ER and 495 nm for green tubulin obtained by tuning the White Light Laser or a 405 nm laser for excitation of Hoechst (all at about 0.3 μW at the sample). Images were acquired at 200/400 Hz with a pixel dwell time of 1.5–2 μs using a HyD (S or X type) detector collecting emission in counting mode except for Hoechst (HyD S1 detector in analog mode).

As previously described for NM-ER in STED REF, a depletion laser at 775 nm was used at 20% (0.21 mW) with the TauSTED mode from the Leica Microsystem and line accumulation of usually 4 lines (2 for *z*-stacks).

Image processing

All images were processed using Leica LasX software with Lightning post processing applied with three iterations. ImageJ 1.54f was also used to post-process images and Igor Pro 8.04 to plot the graphs.

Live cell experiment

Cells were washed once with 250 μL of prewarmed media and stained with ~0.4 μM of NM-ER for at least 30 min. The same procedure was followed for Hoechst at 3 μM (62249, Thermo Scientific) except for the long-term experiment, where 50 nM was used due to impaired mitosis caused by Hoechst. Tubulin was labelled with a GFP using the CellLight Tubulin-GFP, BacMam 2.0 reagent (C10613, Invitrogen). After cells were seeded for 24 h or 48 h (confluency of about 60%), the medium of a well was removed and replaced with a mixture of 150 μL of medium and 25 μL of reagent for another 24 h. Cells were then imaged directly and then fixed. For MitoTracker Green (M7514, Invitrogen), the medium was replaced with a prewarmed medium containing 50 nM of the stain and incubated for 30 min as recommended.

Fixed cell experiment

Cells were washed three times with prewarmed PBS and fixed for 10 min with a prewarmed 4% PFA solution (in PBS). Cells were washed and could be stored at 4 °C until needed. Fixed cells were stained with the same concentrations as for live cell experiments. Cells were stained with WGA-Alexa Fluor 647 (W32466, Invitrogen) diluted in PBS to a final concentration of 2 μg mL^{-1} overnight at 4 °C.

Author contributions

D. F. OS.: conceptualization, funding acquisition, and supervision. A. C. B. and D. F. OS.: writing the original manuscript draft, review and editing. A. C. B.: investigation, methodology, microscopy data acquisition and analysis. M. G.: imaging data analysis, microscopy training, facility management, and reviewing and editing the manuscript.

Conflicts of interest

DFOS has a financial interest in patents granted relating to NIR-fluorophores. All remaining authors declare no conflicts of interest.

Data availability

Data for images contained within the article, supplementary information (SI) and additional examples are accessible from the Zenodo database at DOI: https://doi.org/10.5281/zenodo.15175573.

Supplementary information: additional representative microscopy images shown in Fig. S1–S8 and associated Movies S1–S13 of the figure images. See DOI: https://doi.org/10.1039/d5tb01947h.

Acknowledgements

DFOS gratefully acknowledges funding support from the Irish Government Department of Business, Enterprise and Innovation's Disruptive Technology Innovation Fund. Images are acquired in the RCSI Super Resolution Imaging Consortium funded by Research Ireland (18/RI/5723). A. C. B. acknowledges the Synthesis and Solid-State Pharmaceutical Centre (SSPC) and Research Ireland for funding support, grant number 12/RC/2275_P2.

Notes and references

1 (*a*) C. D. Keating, Aqueous Phase Separation as a Possible Route to Compartmentalization of Biological Molecules, *Acc. Chem. Res.*, 2012, **45**, 2114–2124; (*b*) P. J. Quinn, Lipid–lipid Interactions in Bilayer Membranes: Married Couples and Casual Liaisons, *Prog. Lipid Res.*, 2012, **51**, 179–198.

2 (*a*) T. Harayama and H. Riezman, Understanding the Diversity of Membrane Lipid Composition, *Nat. Rev. Mol. Cell Biol.*, 2018, **19**, 281–296; (*b*) A. Crotta Asis, A. Asaro and G. D'Angelo, Single Cell Lipid Biology, *Trends Cell Biol.*, 2025, **35**, 651–666.

3 (*a*) A. Melero and N. Jiménez-Rojo, Cracking the Membrane Lipid Code, *Cur. Opin. Cell Biol.*, 2023, **83**, 102203; (*b*) J. L. Symons, K.-J. Cho, J. T. Chang, G. Du, M. N. Waxham, J. F. Hancock, I. Levental and K. R. Levental, Lipidomic Atlas of Mammalian Cell Membranes Reveals Hierarchical Variation Induced by Culture Conditions, Subcellular

Membranes, and Cell Lineages, *Soft Matter*, 2021, **17**, 288–297; (*c*) G. van Meer, D. R. Voelker and G. W. Feigenson, Membrane Lipids: Where They Are and How They Behave, *Nat. Rev. Mol. Cell Biol.*, 2008, **9**, 112–124.

4 (*a*) D. Salina, K. Bodoor, D. M. Eckley, T. A. Schroer, J. B. Rattner and B. Burke, Cytoplasmic Dynein as a Facilitator of Nuclear Envelope Breakdown, *Cell*, 2002, **108**, 97–107; (*b*) P. Deolal, J. Scholz, K. Ren, H. Bragulat-Teixidor and S. Otsuka, Sculpting Nuclear Envelope Identity from the Endoplasmic Reticulum During the Cell Cycle, *Nucleus*, 2024, **15**, 2299632; (*c*) J. D. Aitchison and M. P. Rout, A Tense Time for the Nuclear Envelope, *Cell*, 2002, **108**, 301–304.

5 (*a*) E. Anselmo, C. Bonaccorso, G. Gangemi, V. Sancataldo, V. Conti Nibali and G. D'Angelo, Lipid Rafts in Signalling, Diseases, and Infections: What Can Be Learned from Fluorescence Techniques?, *Membranes*, 2025, **15**, 6; (*b*) A. S. Klymchenko, Fluorescent Probes for Lipid Membranes: From the Cell Surface to Organelles, *Acc. Chem. Res.*, 2023, **56**, 1–12; (*c*) Y. Hu, R.-Q. Zhang, S.-L. Liu and Z.-G. Wang, In-situ Quantification of Lipids in Live Cells Through Imaging Approaches, *Biosens. Bioelecton.*, 2023, **240**, 115649; (*d*) A. S. Klymchenko and R. Kreder, Fluorescent Probes for Lipid Rafts: From Model Membranes to Living Cells, *Chem. Biol.*, 2014, **21**, 97–113; (*e*) E. Sezgin, Super-resolution Optical Microscopy for Studying Membrane Structure and Dynamics, *J. Phys.: Condens. Matter*, 2017, **29**, 273001.

6 (*a*) S. Subramaniam, E. Fahy, S. Gupta, M. Sud, R. W. Byrnes, D. Cotter, A. R. Dinasarapu and M. R. Maurya, Bioinformatics and Systems Biology of the Lipidome, *Chem. Rev.*, 2011, **111**, 6452–6490; (*b*) A. Shevchenko and K. Simons, Lipidomics: Coming to Grips with Lipid Diversity, *Nat. Rev. Mol. Cell Biol.*, 2010, **11**, 593–598.

7 J. B. Grimm and L. D. Lavis, Caveat Fluorophore: An Insiders' Guide to Small-Molecule Fluorescent Labels, *Nat. Met.*, 2022, **19**, 149–158.

8 M. Amaro, H. A. Filipe, J. P. Prates Ramalho, M. Hof and L. M. Loura, Fluorescence of Nitrobenzoxadiazole (NBD)-Labeled Lipids in Model Membranes is Connected Not to Lipid Mobility But to Probe Location, *Phys. Chem. Chem. Phys.*, 2016, **18**, 7042–7054.

9 E. M. Storck, C. Özbalci and U. S. Eggert, Lipid Cell Biology: A Focus on Lipids in Cell Division, *Annu. Rev. Biochem.*, 2018, **87**, 839–869.

10 G. E. Atilla-Gokcumen, E. Muro, J. Relat-Goberna, S. Sasse, A. Bedigian, M. L. Coughlin, S. Garcia-Manyes and U. S. Eggert, Dividing Cells Regulate their Lipid Composition and Localization, *Cell*, 2014, **156**, 428–439.

11 (*a*) L. Lu, M. S. Ladinsky and T. Kirchhausen, Cisternal Organization of the Endoplasmic Reticulum During Mitosis, *Mol. Biol. Cell*, 2009, **20**, 3471–3480; (*b*) M. Puhka, H. Vihinen, M. Joensuu and E. Jokitalo, Endoplasmic Reticulum Remains Continuous and Undergoes Sheet-to-Tubule Transformation During Cell Division in Mammalian Cells, *J. Cell Biol.*, 2007, **179**, 895–909; (*c*) D. J. Anderson and M. W. Hetzer, Reshaping of the Endoplasmic Reticulum Limits the Rate for Nuclear Envelope Formation, *J. Cell Biol.*, 2008, **182**, 911–924.

12 A. C. Bourgès, M. Garre, D. Wu and D. F. O'Shea, A STEDable BF_2-Azadipyrromethene Fluorophore for Nuclear Membrane and Associated Endoplasmic Reticulum Imaging, *Membranes*, 2025, **15**, 9.

13 S. Kors and A. L. Schlaitz, Dynamic Remodelling of the Endoplasmic Reticulum for Mitosis, *J. Cell Sci.*, 2024, **137**, jcs261444.

14 (*a*) P. Carravilla, A. Dasgupta, G. Zhurgenbayeva, D. I. Danylchuk, A. S. Klymchenko, E. Sezgin and C. Eggeling, Long-term STED Imaging of Membrane Packing and Dynamics by Exchangeable Polarity-Sensitive Dyes, *Biophys. Rep.*, 2021, **1**, 100023; (*b*) J. Alvelid, M. Damenti, C. Sgattoni and I. Testa, Event-Triggered STED Imaging, *Nat. Met.*, 2022, **19**, 1268–1275.

15 (*a*) D. Wu and D. F. O'Shea, Fluorogenic NIR-probes Based on 1,2,4,5-Tetrazine Substituted BF_2-azadipyrromethenes, *Chem. Commun.*, 2017, **53**, 10804–10807; (*b*) S. Pim, A. C. Bourgès, D. Wu, G. Durán-Sampedro, M. Garre and D. F. O'Shea, Observing Bioorthogonal Macrocyclizations in the Nuclear Envelope of Live Cells Using on/on Fluorescence Lifetime Microscopy, *Chem. Sci.*, 2024, **15**, 14913–14923; (*c*) E. Booth, M. Garre, D. Wu, H. C. Daly and D. F. O'Shea, A NIR-Fluorochrome for Live Cell Dual Emission and Lifetime Tracking from the First Plasma Membrane Interaction to Subcellular and Extracellular Locales, *Molecules*, 2024, **29**, 2474; (*d*) N. Curtin, M. Garre, J.-B. Bodin, N. Solem, R. Méallet-Renault and D. F. O'Shea, Exploiting Directed Self-assembly and Disassembly for Off-to-On Fluorescence Responsive Live Cell Imaging, *RSC Adv.*, 2022, **12**, 35655–35665.

16 (*a*) S. Cheung, D. Wu, H. C. Daly, N. Busschaert, M. Morgunova, J. C. Simpson, D. Scholz, P. A. Gale and D. F. O'Shea, Real-Time Recording of the Cellular Effects of the Anion Transporter Prodigiosin, *Chem*, 2018, **4**, 879–895; (*b*) D. Wu, S. Cheung, M. Devocelle, L. J. Zhang, Z. L. Chen and D. F. O'Shea, Synthesis and Assessment of a Maleimide Functionalized BF_2 Azadipyrromethene Near-infrared Fluorochrome, *Chem. Commun.*, 2015, **51**, 16667–16670; (*c*) D. Wu, H. C. Daly, M. Grossi, E. Conroy, B. Li, W. M. Gallagher, R. Elmes and D. F. O'Shea, RGD Conjugated Cell Uptake Off to On Responsive NIR-AZA Fluorophores: Applications Toward Intraoperative Fluorescence Guided Surgery, *Chem. Sci.*, 2019, **10**, 6944–6956; (*d*) C. Caulfield, D. Wu, I. S. Miller, A. T. Byrne, P. Mac Aonghusa, S. Zhuk, L. Cinelli, E. Bannone, J. Marescaux, S. Gioux, M. Diana, T. L. March, A. L. Vahrmeijer, R. Cahill and D. F. O'Shea, BF_2-Azadipyrromethene Fluorophores for Intraoperative Vital Structure Identification, *Molecules*, 2023, **28**, 2167.

17 B. Griepernau, S. Leis, M. F. Schneider, M. Sikor, D. Steppich and R. A. Böckmann, 1-Alkanols and Membranes: A Story of Attraction, *Biochim. Biophys. Acta, Biomembr.*, 2007, **1768**, 2899–2913.

18 J. Jacquemyn, A. Cascalho and R. E. Goodchild, The Ins and Outs of Endoplasmic Reticulum-Controlled Lipid Biosynthesis, *EMBO Rep.*, 2017, **18**, 1905–1921.

19 J. Liou, M. Fivaz, T. Inoue and T. Meyer, Live-cell Imaging Reveals Sequential Oligomerization and Local Plasma Membrane Targeting of Stromal Interaction Molecule 1 after Ca^{2+} Store Depletion, *Proc. Natl. Acad. Sci. U. S. A.*, 2007, **104**, 9301–9306.

20 G. Zhao, S. Liu, S. Arun, F. Renda, A. Khodjakov and D. A. Pellman, Tubule-sheet Continuum Model for the Mechanism of Nuclear Envelope Assembly, *Dev. Cell*, 2023, **58**, 847–865.

21 S. Güttinger, E. Laurell and U. Kutay, Orchestrating Nuclear Envelope Disassembly and Reassembly During Mitosis, *Nat. Rev. Mol. Cell Biol.*, 2009, **10**, 178–191.

22 D. LaJoie and K. S. Ullman, Coordinated Events of Nuclear Assembly, *Curr. Opin. Cell Biol.*, 2017, **46**, 39–45.

23 M. Vietri, K. O. Schink, C. Campsteijn, C. S. Wegner, S. W. Schultz, L. Christ, S. B. Thoresen, A. Brech, C. Raiborg and H. Stenmark, Spastin and ESCRT-III Coordinate Mitotic Spindle Disassembly and Nuclear Envelope Sealing, *Nature*, 2015, **522**, 231–235.

24 (*a*) S. Otsuka, K. H. Bui, M. Schorb, M. J. Hossain, A. Z. Politi, B. Koch, M. Eltsov, M. Beck and J. Ellenberg, Nuclear Pore Assembly Proceeds by an Inside-Out Extrusion of the Nuclear Envelope, *eLife*, 2016, 5; (*b*) L. Lu, M. S. Ladinsky and T. Kirchhausen, Formation of the Postmitotic Nuclear Envelope from Extended ER Cisternae Precedes Nuclear Pore Assembly, *J. Cell Biol.*, 2011, **194**, 425–440.

25 F. A. Barr and U. Gruneberg, Cytokinesis: Placing and Making the Final Cut, *Cell*, 2007, **131**, 847–860.

26 G. Kunduri, U. Acharya and J. K. Acharya, Lipid Polarization During Cytokinesis, *Cells*, 2022, **11**, 3977.

27 (*a*) L. Capalbo, Z. I. Bassi, M. Geymonat, S. Todesca, L. Copoiu, A. J. Enright, G. Callaini, M. G. Riparbelli, L. Yu, J. S. Choudhary, E. Ferrero, S. Wheatley, M. E. Douglas, M. Mishima and P. P. D'Avino, The Midbody Interactome Reveals Unexpected Roles for PP1 Phosphatases in Cytokinesis, *Nat. Commun.*, 2019, **10**, 4513; (*b*) E. Peterman, P. Gibieža, J. Schafer, V. A. Skeberdis, A. Kaupinis, M. Valius, X. Heiligenstein, I. Hurbain, G. Raposo and R. Prekeris, The Post-abscission Midbody is an Intracellular Signaling Organelle that Regulates Cell Proliferation, *Nat. Commun.*, 2019, **10**, 3181.

28 S. Petry, Mechanisms of Mitotic Spindle Assembly, *Annu. Rev. Biochem.*, 2016, **85**, 659–683.

29 (*a*) M. Glotzer, Cytokinesis: Central Spindlin Moonlights as a Membrane Anchor, *Curr. Biol.*, 2013, **23**, R145–R147; (*b*) D. McCollum, Cytokinesis: The Central Spindle Takes Center Stage, *Curr. Biol.*, 2004, **14**, R953–R955.

30 J. S. Verdaasdonk and K. Bloom, Centromeres: Unique Chromatin Structures that Drive Chromosome Segregation, *Nat. Rev. Mol. Cell Biol.*, 2011, **12**, 320–332.

31 P. Mishra and D. C. Chan, Mitochondrial Dynamics and Inheritance During Cell Division, Development and Disease, *Nat. Rev. Mol. Cell Biol.*, 2014, **15**, 634–646.

32 E. J. Lawrence, E. Boucher and C. A. Mandato, Mitochondria-Cytoskeleton Associations in Mammalian Cytokinesis, *Cell Div.*, 2016, **11**, 3.

33 (*a*) C. J. Gomes, M. W. Harman, S. M. Centuori, C. W. Wolgemuth and J. D. Martinez, Measuring DNA Content in Live Cells by Fluorescence Microscopy, *Cell Div.*, 2018, **13**, 6; (*b*) B. Kalatova, R. Jesenska, D. Hlinka and M. Dudas, Tripolar Mitosis in Human Cells and Embryos: Occurrence, Pathophysiology and Medical Implications, *Acta Histochem.*, 2015, **117**, 111–125.

34 K. Salmina, B. I. Gerashchenko, M. Hausmann, N. M. Vainshelbaum, P. Zayakin, J. Erenpreiss, T. Freivalds, M. S. Cragg and J. Erenpreisa, When Three Isn't a Crowd: A Digyny Concept for Treatment-Resistant, Near-Triploid Human Cancers, *Genes*, 2019, **10**, 551.

35 M. Collot, S. Pfister and A. S. Klymchenko, Advanced Functional Fluorescent Probes for Cell Plasma Membranes, *Curr. Opin. Chem. Biol.*, 2022, **69**, 102161.

36 X. Duan, Q. Tong, C. Fu and L. Chen, Lysosome-Targeted Fluorescent Probes: Design Mechanism and Biological Applications, *Bioorg. Chem.*, 2023, **140**, 106832.

37 H. Tian, A. C. Sedgwick, H.-H. Han, S. Sen, G.-R. Chen, Y. Zang, J. L. Sessler, T. D. James, J. Li and X.-P. He, Fluorescent Probes for the Imaging of Lipid Droplets in Live Cells, *Coord. Chem. Rev.*, 2021, **427**, 213577.

38 K. Neikirk, A. G. Marshall, B. Kula, N. Smith, S. LeBlanc and A. Hinton, MitoTracker: A Useful Tool in Need of Better Alternatives, *Eur. J. Cell Biol.*, 2023, **102**, 151371.

39 (*a*) T. Kondela, J. Gallová, T. Hauß, J. Barnoud, S. J. Marrink and N. Kučerka, Alcohol Interactions with Lipid Bilayers, *Molecules*, 2017, **22**, 2078; (*b*) N. H. Rhys, D. J. Barlow, M. J. Lawrence and C. D. Lorenz, On the Interactions of Diols and DMPC Monolayers, *J. Mol. Liq.*, 2022, **364**, 119963.